DEPENDENCE OF PERMEABILITY VARIATIONS ON THE TEXTILE STRUCTURE

A. Endruweit, A.C. Long, F. Robitaille, C.D. Rudd

School of Mechanical, Materials, Manufacturing Engineering & Management, University of Nottingham, University Park, Nottingham, NG7 2RD, U.K.

ABSTRACT

The global flow behaviour for radial resin injection into a bi-directional non-crimp fabric placed in a flat mould has been simulated implementing a Monte-Carlo-method for generation of local variations in textile properties. Statistical evaluation indicates that with increasing fibre angle variation, the mean value of the normally distributed global permeability, which is determined from the simulated flow front propagation in the mould, decreases continuously, while its standard deviation increases. Mean values and standard deviations of fill times increase continuously. The mould filling patterns are affected especially for high fibre angle variations. Interpretation of the results suggests that the global permeability is mainly determined by the reproducibility of the local fibre configuration, while the dimensions of the unit cell locally affect the flow front shape.

1. INTRODUCTION

In Liquid Composites Moulding (LCM) processes, the impregnation of the textile reinforcement structure with liquid resin is determined by the textile permeability. While various methods for permeability measurement and various approaches for permeability description exist, the high variance of actual permeability values [1,2] is a general problem. This variance is caused by the poor reproducibility of the specified textile properties. Fabrics as delivered by suppliers are in general not completely homogeneous, and the textile structure is affected by gravity and handling of the textiles during storage and transport as well as by cutting and stacking of the fabric layers during preform preparation. Variations in the textile structure cause variations in permeability values. Due to these uncertainties, the mould filling patterns and injection times in LCM processing of actual parts are hard to predict. To optimise the impregnation process and to guarantee the quality of the finished part, it may even be necessary to compensate for uneven preform impregnation by application of process control schemes, which imply control of resin injection gates and vents [3].

Pan et al. [4] investigated and analysed the influence of various factors on measured permeability values for a plain weave and a 0°/90° non-crimp glass fibre fabric based on uni-directional flow experiments. When external influences, such as accidental changes in the experimental conditions, are excluded, the variance of the permeability values of a fabric is caused by local changes in fibre orientation and superficial fabric density. Investigating the distribution of permeability values for a plain weave and a 2x2 twill weave glass fibre fabric and a layered porous reference medium in radial flow experiments, Hoes et al. [5] found that the effect of nesting in a lay-up may also contribute significantly to permeability variations. Both Pan et al. [4] and Hoes et al. [5] found that the principal permeability values of the investigated textiles are normally distributed. However, since the quantitative evaluation of flow experiments implies averaging of local variations in material properties and gives global permeability values, the experimentally determined permeability values characterise quasi-homogeneous materials. The accurate description of global flow for non-uniform materials requires knowledge of the distribution of local properties. De Parseval et al. [6] simulated one-dimensional flow with stochastic and regular local permeability variations to study the effect on the global permeability. They observed that for the one-dimensional case the global permeability is the spatial harmonic mean of the local permeability values. Padmanabhan and Pitchumani [7] performed stochastic analyses of non-isothermal injection processes based on simulation of one-dimensional flow. Unlike Pan et al. and Hoes et al., they assume that the porosity can be described by a normal distribution and the permeability by a log-normal distribution, in which the logarithm of the permeability has a normal distribution. For a

rectangular mould with linear injection gate, Sozer [8] performed flow simulations applying local random permeability variations to observe the effect of preform non-uniformity on mould filling. Random permeability variations of up to ± 35 % are reported to have no significant effect on the flow pattern, while permeability variations in a specific pattern cause a more significant effect on the mould filling results.
With regard to the robust manufacture of composite parts applying LCM processes, this study aims at the prediction of the range of probable outcomes of resin injections, at the determination of the global permeability and its variance and at the estimation of the influence of the textile architecture on the variations in flow propagation for textiles with locally varying properties. The global flow behaviour is described by means of numerical resin flow simulation for the example of radial injection into a flat mould, in which a bi-directional non-crimp fabric is placed. The local variations in textile properties are generated based on a Monte-Carlo-method, which implies the evaluation of normally distributed fibre angles. The fibre angles are stochastically attributed to local domains in the discretised model for numerical resin injection simulation. Information on local fibre orientations allows estimating local fibre density and permeability values based on relatively simple geometrical considerations. The permeability distribution is implemented in the resin injection simulation, which gives the global flow behaviour.

2. LOCAL PERMEABILITY DISTRIBUTION

The fibre angle distribution has been investigated for the example of an unsheared ± 45° non-crimp glass fibre fabric Formax FGE106 [9]. The ideal superficial density of the fabric as specified by the manufacturer is 0.950 kg/m^2, while for the investigated material batch an actual value of 0.936 kg/m^2 has been found. The two layers of uni-directional glass fibres are stitch-bonded using a high-drape stitch construction. The angle θ between the fibre direction and the 90° direction of the fabric, which is expected to coincide with half the angle α between both fibre orientations, has been experimentally determined at various positions on both faces of the fabric by means of photographic imaging and digital image analysis. Statistical evaluation of the data indicates that θ can be described by a normal distribution with a mean value of 42.7° and a standard deviation of 5.6°. Fig. 1 compares the histogram of the observed angle distribution with the corresponding normal distribution indicating satisfactory agreement with a correlation coefficient $R^2 = 0.955$.

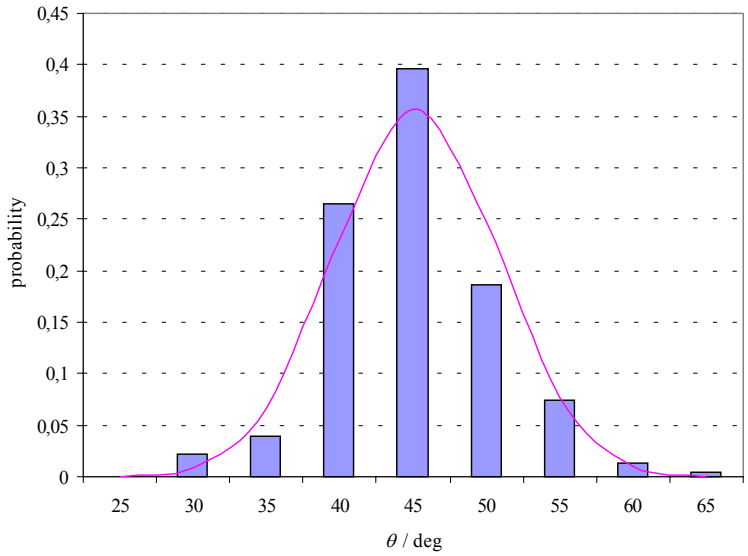

Fig. 1. Angle θ between fibre direction and 90° direction of the fabric: histogram of experimental data and corresponding normal distribution.

For normally distributed fibre angles α with mean value α_0 and variance σ^2, the probability function is

$$P(\alpha)=\frac{1}{\sigma\sqrt{2\pi}}\exp\left(-\frac{(\alpha-\alpha_0)^2}{2\sigma^2}\right) \tag{1}$$

on the domain $\alpha \in (0°,180°)$. The distribution function

$$D(\alpha)=\frac{1}{2}\left(1+\mathrm{erf}\left(\frac{\alpha-\alpha_0}{\sigma\sqrt{2}}\right)\right) \tag{2}$$

with the error function

$$\mathrm{erf}(z)=\frac{2}{\sqrt{\pi}}\int_0^z \exp(-t^2)\,dt \tag{3}$$

describes the probability for the fibre angle to take on a value less than or equal to α. With Eq. (2), values for the normally distributed fibre angle can be generated from uniformly distributed random values D on the interval (0,1) via

$$\alpha=\sigma\sqrt{2}\,\mathrm{erf}^{-1}(2D-1)+\alpha_0 \quad . \tag{4}$$

The inverse error function in Eq. (4) is approximated by a power series. For assignment of properties to domains in the resin flow simulation, which in the following are identified with the finite elements representing the mould, random numbers between 0 and 1 are generated giving exactly one fibre angle α with

$$0°\le\alpha\le180°$$

for each domain. For a given fibre angle, the fibre orientations are described by vectors $\mathbf{e}_{warp}$ and $\mathbf{e}_{weft}$. In the two-dimensional case (x-y-plane), the angles between the fibre orientations of the deformed textile and the reference orientations $\mathbf{e}_x$ and $\mathbf{e}_y$ of the initial fibre configuration are constrained by the condition that the vectors $\mathbf{e}_{warp}$ and $\mathbf{e}_{weft}$ lie within sectors with opening angle $2(90°-\alpha)$, which include $\mathbf{e}_x$ and $\mathbf{e}_y$ as bi-sectors. This condition relates the absolute deviations of both fibre orientations from the initial orientations to the change in angle between the fibre axes. While the fibre orientations are treated as being independent for each finite element ignoring the continuity of the fibre curvature between adjacent elements, the imposed constraints exclude incompatibility of the fibre orientations.

The textile porosity and the permeability tensor are calculated locally implementing a model described by Smith et al. [10], which estimates the permeability of bi-axial fabrics with identical properties in both fibre directions based on the permeabilities of two uni-directional fibre layers. The principal permeability directions of the textile are described as the bi-sectors of the two fibre directions. The principal vectors $\mathbf{e}_1$ and $\mathbf{e}_2$ are calculated from $\mathbf{e}_{warp}$ and $\mathbf{e}_{weft}$. The fibre volume fraction of the bi-directional fibre arrangement is

$$V_f=\frac{n\,S_0}{h\,\rho\sin2\theta} \tag{5}$$

with the number of fabric layers n, the fabric superficial density S_0, the cavity thickness h, the density of the fibre material ρ and the fibre angle

$$2\theta = \alpha \quad . \tag{6}$$

The relation between fibre volume fraction and porosity is

$$\Phi = 1 - V_f \quad . \tag{7}$$

For a layer of uni-directional fibre material, the longitudinal and transversal principal permeability values,

$$k_1 = \frac{R_f^2}{4c_1}\frac{(1-V_f)^3}{V_f^2} \quad \text{and} \quad k_2 = \frac{R_f^2}{4c_2}\frac{(1-V_f)^3}{V_f^2} \quad , \tag{8}$$

are calculated from V_f according to Kozeny-Carman with the fibre radius R_f and the Kozeny-constant c_i for direction i. For any arbitrary flow direction deviating from the fibre axis by an angle θ, the permeability tensor is

$$\begin{pmatrix} k_{xx} & k_{xy} \\ k_{yx} & k_{yy} \end{pmatrix} = \begin{pmatrix} k_1\cos^2\theta + k_2\sin^2\theta & (k_2-k_1)\sin\theta\cos\theta \\ (k_2-k_1)\sin\theta\cos\theta & k_1\sin^2\theta + k_2\cos^2\theta \end{pmatrix} \quad . \tag{9}$$

Assuming identical thickness of the layers and ideal fluid volume exchange between layers, superposition of the permeabilities for both fibre directions (angles θ and $-\theta$) with thickness-weighted averaging gives for the principal permeability values of the fabric

$$K_1 = k_{xx} \quad \text{and} \quad K_2 = k_{yy} \quad . \tag{10}$$

3. INJECTION SIMULATION

Radial injection experiments with central injection gate in a square shaped tool with an edge length of 0.5 m and an injection gate radius R_0 of 5 mm have been simulated for randomly assigned fibre angle distributions of the fabric. The equations describing the flow of a viscous liquid through a porous medium considering conservation of the fluid mass are solved based on a non-conforming finite element method [11], which is implemented in the PAM-RTM software. Discretising the flow domain, a mesh with 1708 elements has been generated (Fig. 2). A value of 0.1 Pa·s has been given for the viscosity η of the injected resin. The injection pressure Δp has been set to 10^5 Pa. For the superficial density of the fabric S_0 [9], the number of fabric layers n, the cavity height h, the fibre density ρ, the Kozeny constants c_1 and c_2 [12] and the fibre radius R_f, the values listed in Table 1 have been specified.

Table 1. Input parameters for calculation of local porosity and permeability values.

S_0 / kg/m^2	n	h / m	ρ / kg/m^3	c_1	c_2	R_f / m
0.936	4	0.0044	2600	0.017	0.040	$7.5\cdot10^{-6}$

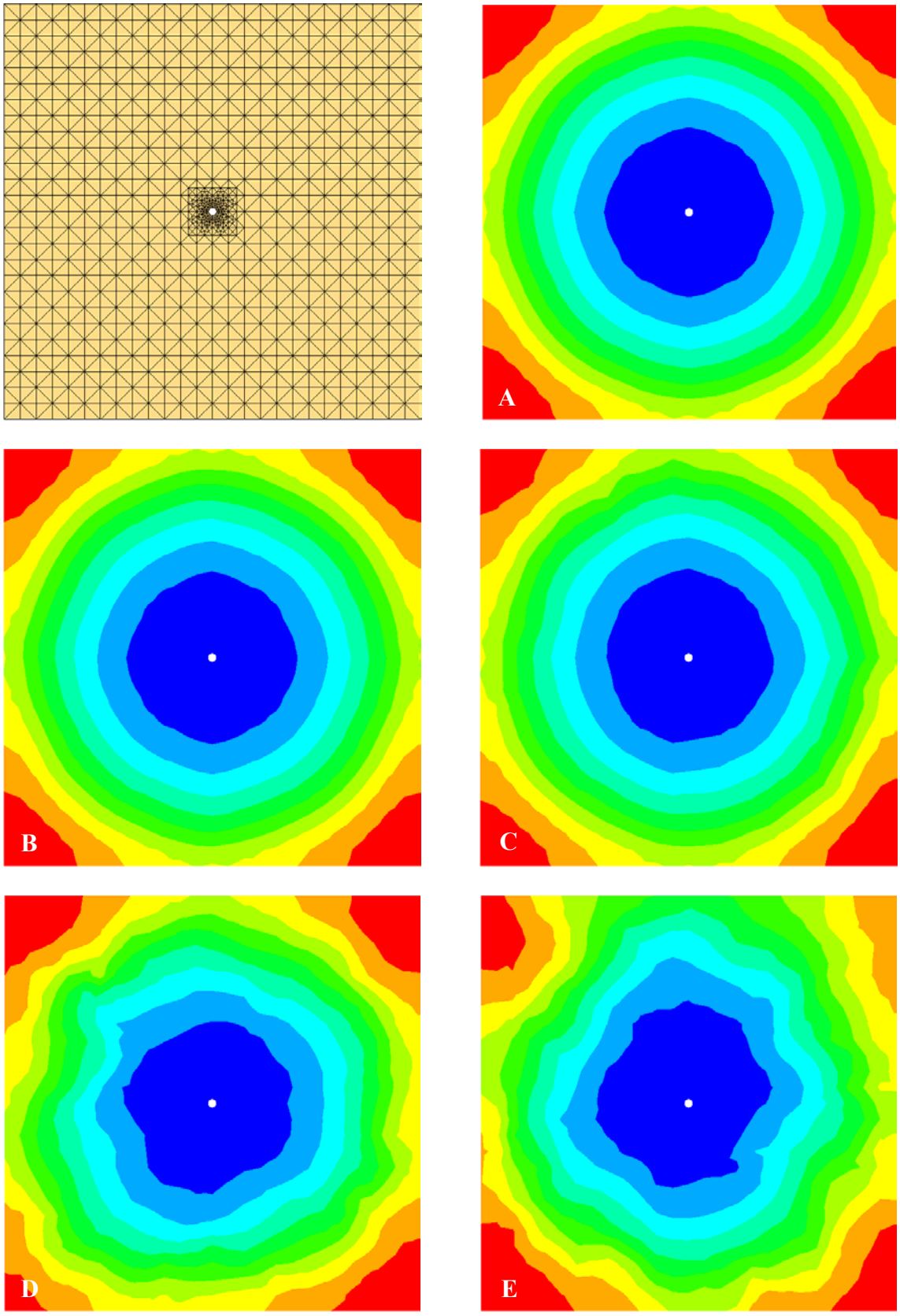

Fig. 2. Finite element model for simulation of radial injection and examples for the flow front position as function of time. A: homogeneous fabric, fill time 59.7 s; B: $\sigma = 10°$, fill time 62.6 s; C: $\sigma = 20°$, fill time 75.1 s; D: $\sigma = 30°$, fill time 115 s; E: $\sigma = 40°$, fill time 191 s.

For a mean fibre angle α_0 of 90° and each of the standard deviations σ of 10°, 20°, 30° and 40°, 100 fibre angle distributions have been generated. With the generated random distributions of fibre angles and vectors representing the fibre axes, principal permeability vectors and local porosity and permeability values have been determined for each finite element. For each data set, resin injection has been simulated. In addition, injection into a homogeneous fabric has been simulated for comparison. Examples of the flow front shapes as function of time are shown in Fig. 2.

In Fig. 2, the reference image with the homogeneous fabric (Fig. 2A) shows slight deviations in flow front shape from the expected circular shape due to discretisation effects. For a standard deviation in fibre angles of 10°, hardly any difference in flow front shape can be observed (Fig. 2B). Fig. 2C (standard deviation of 20°) shows a more significant deviation in flow front shape from the shape for the homogeneous fabric, while the filling patterns in Fig. 2D and 2E (standard deviations of 30° and 40°) are both highly distorted. More detailed evaluation of the flow front propagation indicates that the last corner of the tool to be filled varies from simulation to simulation. While for the homogeneous fabric all four corners are filled simultaneously, with increasing fibre angle variation they are basically filled successively. Evaluation of the flow velocity distribution indicates that the flow paths are not following straight radial lines.

The quantitative evaluation and comparison of various simulations is based on the injection times for complete filling of the mould t_{fill}. In addition, the flow can be characterised using virtual pressure sensors on the finite element model of the injection geometry. The change in slope of the recorded curve of the pressure as function of time indicates that the fluid has reached the virtual sensor at time t_{vs}. For each standard deviation of fibre angles, averaging of the flow fronts over 100 simulations gives an isotropic solution with no preferred flow direction. Thus, the time t_{vs} for the flow front to reach a virtual sensor at a radial distance R = 250 mm from the centre of the geometry can be used to calculate

$$\frac{k}{\Phi} = \left(\left(\frac{R}{R_0} \right)^2 \left(2 \ln \left(\frac{R}{R_0} \right) - 1 \right) + 1 \right) \frac{\eta R_0^2}{4 \Delta p \, t_{vs}} \quad , \tag{11}$$

which is derived from integration of Darcy's law in two dimensions [13]. The isotropic quantity k/Φ characterises the actual resin flow velocity

$$\mathbf{v}_r = -\frac{k}{\eta \Phi} \nabla p \quad . \tag{12}$$

Separate treatment of the permeability is not possible, since the average values of both permeability and porosity are unknown.

In Table 2, results for t_{fill}, t_{vs} and k/Φ from statistical evaluation of the simulations are listed (average value ± standard deviation). Both t_{fill} and t_{vs} show similar trends. Mean values and standard deviations increase continuously with increasing variation of the fibre orientations, which is characterised by σ. The standard deviations of the fill times correspond to relative variations of ± 0.5 % (σ = 10°), ± 2.1 % (σ = 20°), ± 5.6 % (σ = 30°) and ± 7.6 % (σ = 40°). This increase is caused by local reductions in porosity and permeability according to Eqs. (5) to (10). With respect to k/Φ, the mean value decreases continuously, while the standard deviation increases. For k/Φ, the derived relative variations are ± 0.9 % (σ = 10°), ± 3.8 % (σ = 20°), ± 10.8 % (σ = 30°) and ± 18.1 % (σ = 40°).

Table 2. Injection time t_{fill} for complete filling of the mould; time t_{vs} for the flow front to reach a virtual sensor at $R = 0.25$ m; k/Φ derived according to Eq. (11).

σ	t_{fill} / s	t_{vs} / s	k/Φ / 10^{-10} m^2
0°	59.7	43.4	24.58
10°	62.4 ± 0.3	44.9 ± 0.4	23.76 ± 0.22
20°	75.4 ± 1.6	53.7 ± 2.0	19.89 ± 0.75
30°	113.1 ± 6.3	77.8 ± 8.3	13.86 ± 1.50
40°	190.8 ± 14.5	130.1 ± 22.6	8.45 ± 1.53

In Fig. 3, the distribution of values for k/Φ and the corresponding normal distribution, which has been determined from the values in Table 2, are compared for the example with $\sigma = 30°$. The correlation coefficient, which characterises the quality of the correlation between the original values and the normal distributions, is $R^2 = 0.908$.

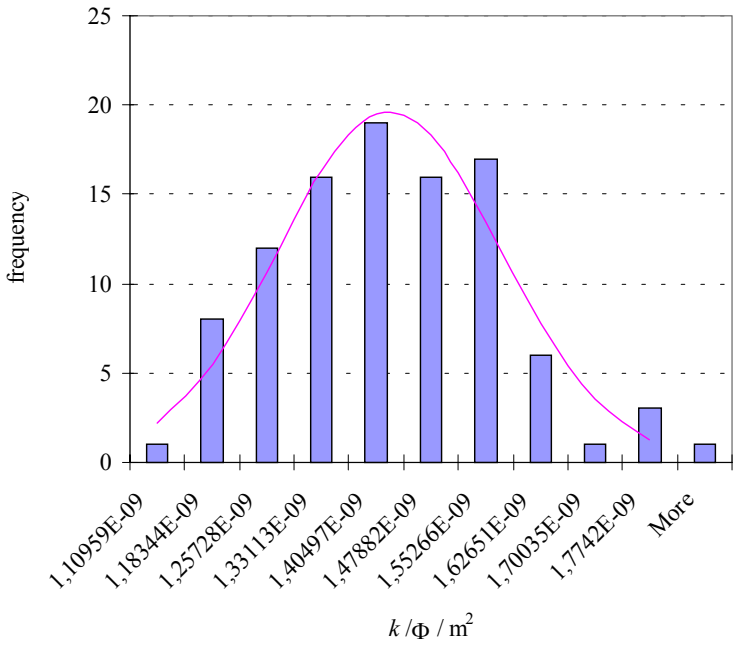

Fig. 3. Distribution of k/Φ for $\sigma = 30°$; histogram and corresponding normal distribution.

All simulations have been repeated for a finer discretisation of the geometry with 3028 triangular elements. In general, the development of the filling patterns with increasing standard deviation of the fibre angles for the fine mesh shows a similar trend as for the coarse mesh. Especially for standard deviations of the fibre angles of 30° and 40°, qualitative comparison of the flow front shapes shows more uneven filling patterns for the coarse mesh. Evaluation of simulation results for the fine mesh gives relative variations of the fill times of ± 0.3 % ($\sigma = 10°$), ± 1.9 % ($\sigma = 20°$), ± 4.6 % ($\sigma = 30°$) and ± 7.6 % ($\sigma = 40°$). The relative variations of k/Φ are ± 0.7 % ($\sigma = 10°$), ± 3.0 % ($\sigma = 20°$), ± 8.2 % ($\sigma = 30°$) and ± 14.2 % ($\sigma = 40°$). Quantitative comparison of the results for the fine mesh and the coarse mesh indicates that for the reference configuration of the homogeneous fabric, the fill time for the coarse mesh is 1.4 % higher, the time to reach the virtual sensor is 3.3 % higher, and k/Φ is 3.1 % lower. The coarse mesh in general shows increased fill times and reduced values of k/Φ. All

standard deviations are increased. Considering the influence of the discretisation on the results for the reference configuration, the influence of the mesh density on t_{fill} and k/Φ is less significant than the influence of the values for σ.

4. DISCUSSION

From the material parameters listed in Table 1, a porosity value $\Phi = 0.67$ and an isotropic permeability value $k = 16.75 \cdot 10^{-10}$ m^2 for the homogeneous reference configuration are calculated applying Eqs. (5) to (10). For k/Φ, this gives a theoretical value of $24.90 \cdot 10^{-10}$ m^2. The value determined from the numerical experiment, $24.58 \cdot 10^{-10}$ m^2, differs by – 1.3 % from this theoretical value, which indicates that the simulation is consistent with the analytical solution of the flow problem given in Eq. (11). For high local variations in the fibre angles, the uneven flow front (as e.g. in Fig. 2E) may reach the boundary of the flow domain before the virtual sensor is reached. This again affects the pressure distribution within the mould and thus the time t_{vs} for the flow front to reach the sensor. To quantify this effect, injection simulations with $\sigma = 40°$ have been repeated for a vented outer boundary of the flow domain (pressure kept constant at 0 Pa). For this boundary condition, the pressure increase after the flow front reaches the mould walls is avoided. The results indicate that the average time t_{vs} in this case is increased by 6 % and the average value k/Φ is decreased by 9 % compared to the values listed in Table 2. These changes are smaller than the calculated relative standard deviations of 17 % for t_{vs} and 18 % for k/Φ and thus are not considered significant. Quantitative evaluation of the simulation results based on the readings of the virtual pressure sensor as discussed above is justified even if the pressure distribution and the flow velocity are locally disturbed.

Visual observation of local permeability variations in unsaturated flow experiments suggests that the architecture of textile fabrics can be characterised by the dimensions of the unit cell and the reproducibility of the fibre configuration, which is related to the shear stiffness and the locking angle. Fig. 4 shows typical flow front shapes for radial injection into an 8-harness satin weave fabric, 296 g/m^2, and a 2x2 twill weave fabric, 880 g/m^2, both sheared to achieve a fibre angle of 75° [14]. For the satin weave fabric, the flow front shape is almost perfectly elliptical, because the fabric is made of fine fibre tows, giving a relatively homogeneous porosity and permeability distribution. The twill weave fabric is made from thick fibre tows, giving a more inhomogeneous porosity and permeability distribution. In addition, the mobility of the fibres, which is related to the minimum fibre angle α_{min} that can be achieved by shearing, is higher for the twill weave fabric ($\alpha_{min} \approx 55°$) than for the satin weave fabric ($\alpha_{min} \approx 75°$). This implies that the reproducibility of the fibre configuration in the twill weave fabric is lower than in the satin weave fabric. With decreasing reproducibility, the variance of local permeability values increases. Thus, the actual flow front shape deviates significantly from a perfect ellipse due to the coarse structure of the fabric and the relatively high local variations of the fibre configuration.

For the injection simulation, the fibres are described as being piecewise straight on the domains of the finite elements. Relating the element size to the dimensions of the textile unit cell and the fibre angle variation to the reproducibility of the fibre structure, the results of the simulations with different mesh densities indicate that the dimensions of the unit cell have a less significant influence on variations of the average global permeability than the shear behaviour. Nonetheless, the simulated flow front contours are in general more even for the fine mesh, i.e. for textiles with fine structure, which is again in agreement with the interpretation of Fig. 4.

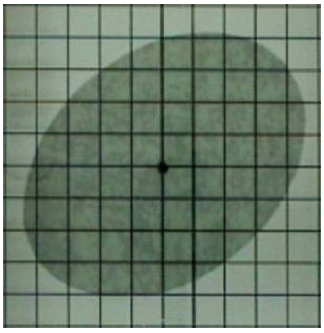

satin weave, 296 g/m^2, $\alpha = 75°$

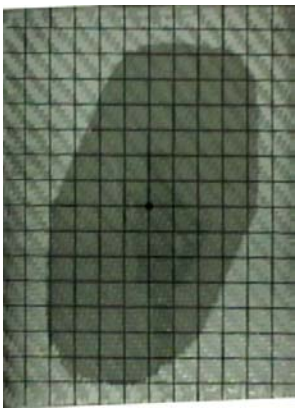

twill weave, 880 g/m^2, $\alpha = 75°$

Fig. 4. Qualitative comparison of typical flow front shapes for woven fabrics of different architecture [14].

For the unsheared glass fibre fabric Formax FGE106, the experimentally observed standard deviation of 5.6° in θ corresponds to a standard deviation of 7.9° in α. For this case, linear interpolation of the results listed in Table 2 gives a fill time of (61.8 ± 0.2) s (relative variation ± 0.3 %). The value for k/Φ is (23.93 ± 0.17)·10^{-10} m^2 (relative variation ± 0.7 %). A series of 30 unsaturated injection experiments with radial injection at a constant flow rate has been carried out on the same material to determine the global permeability. Engine oil with given viscosity(temperature) characteristics has been used as test fluid. Evaluation of the experiments is based on measurement of the pressure as function of time for an array of pressure transducers in the mould [15]. Variations in the mass of the unsheared textile specimens of ± 0.3 % indicate that the global superficial density is relatively constant. The fibre volume fraction in the mould is approximately constant at 0.37. While the theoretical value for k is 10.80·10^{-10} m^2, the experimental results suggest a value of (10.12 ± 2.56)·10^{-10} m^2 (relative variation ± 25 %). The agreement between experimental mean value and theoretical value is good (deviation - 6.3 %). The experimental variation, while in the same range as documented e.g. by Hoes et al. [5], is much higher than predicted based on the simulation results. While the limitations of the approach for numerical modelling, which implies that all fabric layers in the preform show identical behaviour and that there are no inter-layer effects such as nesting, causes differences in permeability variation, uncertainties in the experimental procedure for permeability measurement have a more significant influence.

5. CONCLUSIONS

The global flow behaviour for radial resin injection into a bi-directional non-crimp fabric placed in a flat mould has been simulated considering local variations in textile properties. Local fibre density and permeability values have been estimated for normally distributed fibre angles with various standard deviations. Predicting the range of probable outcomes of resin injections in terms of fill times and filling patterns, mean values and standard deviations of times for complete filling of the mould have been found to increase continuously with increasing fibre angle variations. The flow front shapes for low fibre angle variations do not differ by much from the shape for homogeneous material, while for high variations, they are highly distorted. In agreement with the increase in fill times, the mean value of the porosity related global permeability, which is determined from the simulated flow front propagation in the mould, decreases continuously. Its standard deviation increases with increasing fibre angle variations. The global permeability values can be described by a normal distribution. For estimation of the influence of the textile architecture on the variations in flow propagation for

non-uniform textiles, it is assumed that the dimensions of the textile unit cell can be related to the mesh density in the flow simulations and the local reproducibility of the fibre structure to the imposed fibre angle variations. The simulation results suggest that the global permeability is mainly determined by the reproducibility, i.e. the fabric shear behaviour, while the dimensions of the unit cell locally affect the flow front shape.

ACKNOWLEDGEMENT

This research was supported by the Engineering and Physical Sciences Research Council, Dowty Propellers, ESI Software, Ford Motor Company Ltd. and Formax UK Ltd.

References

1. **Lundström, T.S., Stenberg, R., Bergström, R., Partanen, H, Birkeland, P.A.**, "In-plane permeability measurements: a nordic round-robin study", *Compos Part A-Appl S*, **31** (2000), 29-43.
2. **Luo, Y., Verpoest, I., Hoes, K., Vanheule, M., Sol, H., Cardon, A.**, "Permeability measurement of textile reinforcements with several test fluids", *Compos Part A-Appl S*, **32** (2001), 1497-1504.
3. **Barooah, P., Berker, B., Sun, J.Q.**, "Integrated Switching and Feedback Control for Mold Filling in Resin Transfer Molding", *J Manuf Sci E-T ASME*, **123** (2001), 240-247.
4. **Pan, R., Liang, Z., Zhang, C., Wang, B.**, "Statistical Characterization of Fiber Permeability for Composite Manufacturing", *Polym Composite*, **21**/6 (2000), 996-1006.
5. **Hoes, K., Dinescu, D., Vanheule, M., Sol, H., Parnas, R.S., Belov, E., Lomov, S.**, "Statistical distribution of permeability values of different porous materials", *Proceedings of the Tenth European Conference on Composite Materials*, Brugge (2002).
6. **de Parseval, Y., Valery Roy, R., Advani, S.G.**, "Effect of local variations of perform permeability on the average permeability during resin transfer molding of composites", *Proceedings of the 53rd Annual Technical Conference of the Society of Plastics Engineers*, Boston (1995), 3040-3044.
7. **Padmanabhan, S.K., Pitchumani, R.**, "Stochastic modelling of nonisothermal flow during resin transfer molding", *Int J Heat Mass Tran*, **42** (1999), 3057-3070.
8. **Sozer, E.M.**, "Effect of preform non-uniformity on mold filling in RTM process", *International SAMPE Technical Conference Series*, **33** (2001), 176-189.
9. **Andrews, R.A.**, "Real life process simulation – Predicting the range of outcomes during composites manufacturing", BEng Individual Project Report, University of Nottingham (2003).
10. **Smith, P., Rudd, C.D., Long, A.C.**, "The effect of shear deformation on the processing and mechanical properties of aligned reinforcements", *Compos Sci Technol*, **57** (1997), 327-344.
11. **Trochu, F., Gauvin, R., Gao, D.M.**, "Numerical Analysis of the Resin Transfer Molding Process by the Finite Element Method", *Adv Polym Tech*, **12**/4 (1993), 329-342.
12. **Long, A.C., Blanchard, P.J., Rudd, C.D., Smith, P.**, "The development of an integrated process model for liquid composite moulding", *Compos Part A-Appl S*, **29** (1998), 847-854.
13. **Adams, K.L., Russel, W.B., Rebenfeld, L.**, "Radial Penetration of a Viscous Liquid into a Planar Anisotropic Porous Medium", *Int J Multiphas Flow*, **14**/2 (1988), 203-215.
14. **Endruweit, A., Ermanni, P.**, "The In-Plane Permeability of Sheared Textiles. Experimental Observations and a Predictive Conversion Model", *Compos Part A-Appl S*, **35** (2004), 439-451.
15. **Robitaille, F., Long, A.C., Rudd, C.D., Souter, B.J.**, "The measurement of in-plane permeability for sheared performs", *Proceedings of CADCOMP 98, Computer Methods in Composite Materials VI*, Montreal (1998), 495-504.